Available online at www.sciencedirect.com
ScienceDirect
Catalysis Today 133–135 (2008) 113–119
CATALYSIS TODAY
www.elsevier.com/locate/cattod

Preparation of alumina–titania nanofibers by a pH-swing method

José Antonio Muñoz-López, José Antonio Toledo, José Escobar, Esteban López-Salinas *

Instituto Mexicano del Petróleo, Eje Lázaro Cardenas 152, CP 07730, México, D.F., Mexico

Available online 1 February 2008

Abstract

Fibrillar Al_2O_3–TiO_2 were obtained by a pH-swing method by varying the pH from 2 to 8, and repeating this range (e.g. a cycle) several times, in combination with different ways to incorporate titanium oxisulfate. Depending on the stage in which Ti-oxisulfate is added to the alumina, large anatase aggregates or very dispersed TiO_2 domains were obtained on/in alumina nanofibers. Thus, when using a co-precipitation method in combination with pH-swing between pH 2 and 8, with six pH cycles, a high TiO_2 dispersion can be obtained, as indicated by Raman spectroscopy and X-ray diffraction. On the other hand, when adding Ti-oxysulfate at the end of the pH-swing procedure, though alumina nanofibers were formed, anatase was predominantly located as large particles in the interfibrillar voids. Specific surface area and total pore volume of nanofibrillar Al_2O_3–TiO_2 were around 300 m^2/g and 1 cm^3/g, respectively, after calcining at 500 °C. The highly disordered intertwined fibrils favored high pore volume values, even upon calcinations at 500 °C.

Keywords: Alumina; Alumina–titania support; pH-swing method; Nanofibers

1. Introduction

The synthesis of materials with nanoscale dimensions and structure is of great interest and importance in materials science and nanotechnology [1,2]. Particularly, alumina nanofibers have great potential applications as adsorbents, catalysts support, composite materials, and ceramics, among others. In the last years, several studies on alumina nanofibers formation have been reported [3–5].

In recent studies, Zhu et al. [6] obtained alumina nanofibers by precipitating sodium aluminate in a 5N acetic acid solution and PEO as surfactant, at hydrothermal conditions for 8 h and further calcinations at 500 °C. The authors claim that their preparation method can affect the growth direction of boehmite crystals and the final alumina crystals morphology, yielding fibers of average 3–4 nm wide and 30–60 nm long. Zhang et al. [7] found a general route for mesostructured fibrillar alumina, in which the key is the use of meso-structured surfactants during the aluminum cation hydrolysis. In general, their synthesis comprised aluminum hydroxide precipitation and ageing in mother aqueous solution with the surfactant at 80 °C for 6 h and later a 48 h hydrothermal treatment. The final material was dried and calcined at 550 °C for 4 h, showing specific areas between 299 and 370 m^2/g. Gevert and Ying [8] synthesized γ-aluminas with fibrillar morphology using a basic aluminum chloride water solution. During the crystallization of basic chlorohydrol to convert aluminum hydroxides into thin fibers, initial ''wrinkle sheet'' particles, which later transformed into a ''leaf form'' and lastly into a fibrillar form, were detected. These fibers were in average 500 nm long and 50 nm wide. After a 950 °C thermal treatment, this fibrillar alumina showed specific surface area of 121 m^2/g and a pore volume of 0.60 cm^3/g. Typical catalysts (Ni and Mo being the active phases), for the hydroconversion of heavy hydrocarbons were prepared using these alumina nanofibers as support. These catalysts showed better results on intrinsic activity of hydrodemetallization and longer life-time in the hydroconversion of atmospheric residua, in comparison with a commercial NiMo catalyst on a non-fibrillar alumina.

On other hand, in an Al_2O_3–TiO_2 mixed oxide system, the incorporation of TiO_2 to alumina is known to increase the acidity of the resulting mixed oxide, depending strongly on the preparation method and the titania concentration [9]. When using TiO_2 as a support of NiMo catalysts, initial catalytic activity in hydrodesulfurization reactions is much higher than that on catalysts based on pure alumina [10]. One of the main

* Corresponding author.
E-mail address: esalinas@imp.mx (E. López-Salinas).

0920-5861/$ – see front matter © 2008 Published by Elsevier B.V.
doi:10.1016/j.cattod.2007.12.044

inconveniences of using TiO_2 as a catalyst support is its low specific surface area (50–60 m^2/g) and pore volume (~0.3 cm^3/g). One approach to overcome these textural disadvantages is to disperse TiO_2 on a given alumina support. Therefore, the use of alumina–titania as a catalyst support is a good alternative to improve hydrotreating catalysts performance, as long as high TiO_2 dispersions are achieved [11–13]. To our knowledge, studies on fibrillar alumina–titania mixed oxides have not been reported. The importance of fibrillar alumina morphology lies on its inter-fibrillar pores, which favor the diffusion and eventual transformation of huge refractory asphaltene and Ni and/or V porfirinic molecules contained in oil residua, which represent one of the most difficult hydrocarbons to transform in oil hydrotreatment reactions, and contribute enormously to deactivation of catalysts active sites [8].

We have found that by implementation of a pH-swing method, it is possible to obtain boehmite alumina with fibrillar morphology [14]. This pH-swing method was first reported by Ono et al. [15] and consisted on swinging the pH value from acid to basic pH region which corresponded to the limits of the U-shaped solubility curve of alumina. As a result, Ono et al. disclosed a method to control pore size and pore size distribution of aluminas, simply by varying the number of times (swings) a pH value was swung. However, these authors overlooked that in certain conditions, pH-swing method can afford alumina nanofibers.

In this study, we aimed at obtaining alumina–titania nanofibers by a pH-swing method, combined with three different ways to incorporate a TiO_2-precursor on Al_2O_3 (co-precipitation, deposition and stepwise deposition). The overall purpose was to reveal a method in which TiO_2 was highly dispersed.

2. Experimental

2.1. pH-swing method

Both single alumina (A6pHs, obtained after six pH cycles as in Fig. 1) and Al_2O_3–TiO_2 mixed oxides were synthesized following a modified pH-swing method [15]. A general preparation flow diagram is displayed in Fig. 1. All preparations were carried out at constant 60 ± 3 °C temperature. The initial pH-swing cycle was as follows: in a glass vessel containing 200 ml of aqueous $Al_2O_3{\cdot}NaO_2$ (basic pH), an aqueous $Al_2(SO_4)_3{\cdot}18H_2O$ solution (acid pH) was poured until reaching pH 2. Then, the white precipitate was kept for 5 min and then another portion of aqueous $Al_2O_3{\cdot}NaO_2$ solution was added until reaching stable pH 8 in the reaction mixture, and aged for 5 min. This stage is the first pH-swing cycle, and can be repeated a number of times to affect the textural properties. In this work, we carried out six pH-swing cycles in all synthesis, maintaining all other conditions constant. After completing six pH-swing cycles, the resulting slurry was filtered in Buchner-type funnel connected to a vacuum pump. The filtered white cake was repeatedly removed and washed by ion-exchange during 120 min for each washing, at ambient temperature. The ion-exchange solution was 0.1N $(NH_4)_2CO_3$ and was repeated

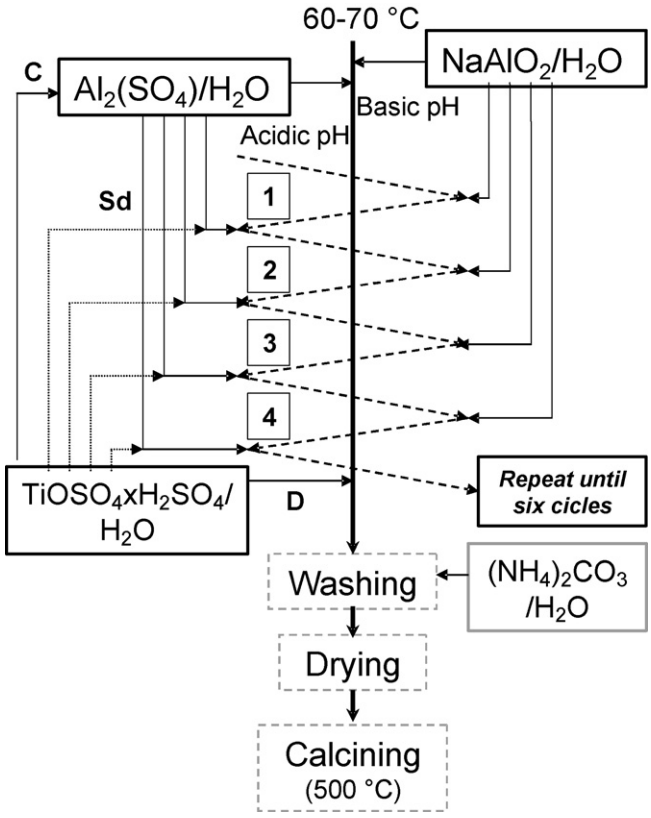

Fig. 1. Preparation flow diagram of alumina and alumina–titania by a pH-swing method and the different incorporation techniques of titania. C: co-precipitation; D: deposit; Sd: stepwise deposit.

four times with fresh solution in each sample. This washing method replaces remaining ions such as $SO_4^{=}$ and/or Na^+ by $CO_3^{=}$ and/or NH_3^+ ions, respectively, with a view to reduce undesirable residues in the calcination step. After this, the wet cake was transferred to a stove and dried at 120 °C for 18 h. Then, the material was calcined in a furnace at 5 °C/min until 500 °C and kept for 4 h.

2.2. TiO_2 incorporation

As mentioned above, three TiO_2-precursor incorporation methods were used: (i) co-precipitation, (ii) deposition, and (iii) stepwise deposition (see Fig. 1, to distinguish these three methods). In all mixed oxides, $TiOSO_4{\cdot}xH_2SO_4{\cdot}xH_2O$ ($TiOSO_4$) was used as a TiO_2 source. As well, in all alumina–titania preparations a nominal 15 wt.%, based on alumina, was estimated. For comparison purposes in some examples, commercial anatase Hombitek K was used. *Co-precipitation method* (*C*)*:* co-precipitation consisted in adding the $TiOSO_4$ admixed with the aluminum sulfate acid solution. The sample obtained by this method was referred to as Cs5. *Deposition method* (*D*)*:* in the deposition method, $TiOSO_4$ was added until the end of the six pH-swing cycles, that is after the formation of alumina. These samples were referred to as Ds5. *Stepwise deposition method* (*Sd*)*:* In this method, when finishing each pH-swing cycle, $TiOSO_4$ solution was added in partial quantities. In other words, total quantity of this

Table 1
Textural properties and TiO_2 content of alumina–titania materials and those of single alumina A6pHs calcined at 500 °C

Sample	TiO_2 addition technique	TiO_2 (wt.%)	Specific area (m^2/g)	Pore volume (cm^3/g)	Pore size (nm)
Cs5	Co-precipitation	8.9	337	0.57	6.8
Sd5	Stepwise deposition	10.8	330	1.05	12.8
Ds5	Deposition	13.7	311	1.02	13.1
A6pHs	None	0	298	0.99	13.3

solution was separated in six equal portions. The sample obtained by this technique will be referred to as Sd5.

2.3. Materials characterization

2.3.1. Textural analysis

All textural properties were determined on calcined materials at 500 °C, using a Micromeritics Digisorb ASAP-2405 equipment. Specific surface areas were calculated by a Brunauer–Emmet–Teller equation, based on the adsorption isotherm of N_2 at −196 °C. Pore size distributions were obtained by a Barret–Joyner–Hallenda method (BJH) on the desorption cycle.

2.3.2. X-ray diffraction (XRD)

Powdered materials were characterized by XRD using a Siemens D-5005 equipment with a digital record system and Cu Kα (λ = 1.5406 Å) radiation, where $K\alpha_2$ was eliminated by a Diffract Plus V 1.01. software. Diffraction intensity was measured in 2θ range between 10° and 80°, with a 0.03° step each 8 s for point.

2.3.3. Chemical analysis

TiO_2 content in pH-swing alumina–titania solids was determined by ion-coupled plasma spectroscopy (ICP) in Perkin-Elmer OPTIMA 3200DV equipment. Samples (0.3 g) were dissolved in nitric acid and transferred to the nebullization camera using a peristaltic pump at 1 cm^3/min, using Ar as carrier gas.

2.3.4. Transmission electronic microscopy (TEM)

TEM analysis was performed using JEOL 2010F Microscope operating at 200 kV. Samples were pulverized and suspended in isopropanol at ambient temperature with ultrasonic stirring, and then an aliquot was dropped in a 3 mm carbon–copper grid.

2.3.5. Raman spectroscopy

Raman spectra were recorded at ambient temperature on samples calcined at 500 °C, in a Yvon Jobin Horiba T64000 spectrometer equipped with a Olympus BX-41 confocal microscopy, 514.5 nm laser beam and 15 mW power. This spectrometer was equipped with a CCD detector.

2.3.6. UV–visible analysis (UV–vis)

UV–vis diffuse reflectance spectra were obtained in a Varian Cary-4 UV-v spectrometer with a Harrick-Scientific Praying-Mantis special accessory for diffuse reflectance.

3. Results and discussion

Textural properties of Al_2O_3–TiO_2 and those of single alumina (A6pHs) materials, after calcining at 500 °C, are shown in Table 1. The specific surface area of A6pHs was 298 m^2/g, while Al_2O_3–TiO_2 materials showed values between 311 and 337 m^2/g, indicating a relative increase in specific area values in spite of the different preparation methods and the presence of TiO_2. The highest surface area (337 m^2/g) was obtained in the Cs5 sample, while the lowest one was 311 m^2/g, in Ds5 prepared by deposition. In contrast, average pore size and total pore volume in the Cs5 material were the lowest ones (6.8 nm and 0.57 cm^3/g, respectively) in comparison with those of the other Al_2O_3–TiO_2 materials which were in average 13 nm and 1.02 cm^3/g, respectively.

In the pore size distribution curves (PSDCs) shown in Fig. 2, it can be observed that pore size in Cs5 shifted towards smaller sizes in comparison with the other samples; besides, the shape of PSDC is more narrow, indicating that pore sizes are more uniform than the other samples. It is clear then that incorporation of TiO_2 by a co-precipitation method yields texturally different Al_2O_3–TiO_2 materials than those obtained by the other methods and even different than reference single alumina. In other words, incorporation of TiO_2 either by deposition or stepwise deposition yields Al_2O_3–TiO_2 materials with similar textural properties than A6pHs.

The shape of N_2 adsorption–desorption isotherms indicate that all materials are mesoporous, as shown in Fig. 3; but a

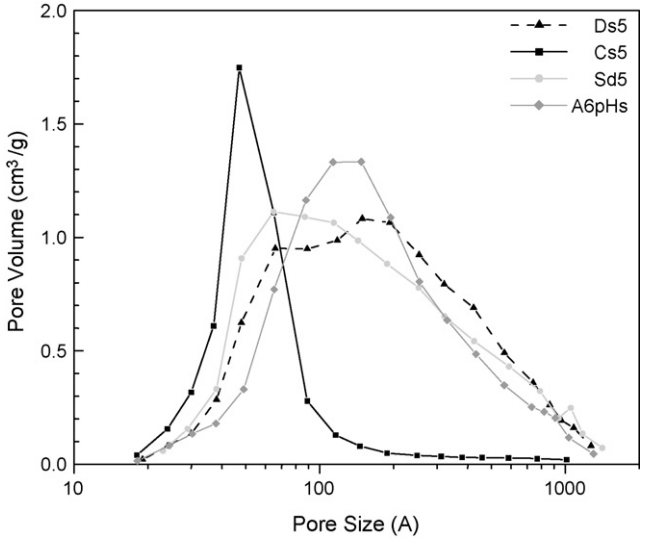

Fig. 2. Pore size distribution curves of single A6pHs alumina and those of alumina–titania materials calcined at 500 °C.

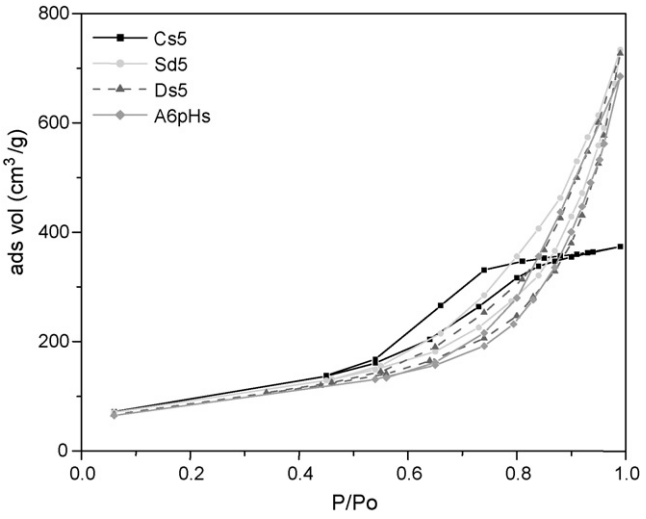

Fig. 3. Nitrogen adsorption–desorption isotherms from single A6pHs alumina and those of alumina–titania materials calcined at 500 °C.

difference between Cs5 sample and the others is clear. The hystheresis loop of Cs5 is H2-type, as indicated by the IUPAC classification, which derive from complex and interconnected porous structures with different shapes and sizes. On the other hand, A6pHs alumina, Ds5 and Sd5 show similar H3-type hystheresis loops among them, being characteristic of materials made up of aggregates of particles with plaques or fiber shapes yielding slit-like pores [16].

The morphology of A6pHs and Al_2O_3–TiO_2 materials was examined by TEM and their images are shown in Fig. 4. All samples showed clear fibrillar morphologies. The fibrils are mainly disordered and very few bundles were found where fibrils were parallel to each other. In A6pHs fibrils are in average 90 nm long × 6 nm wide. Ds5 and Sd5 showed fibrils with similar dimensions as those in A6pHs, but additionally some plaque-like regions (rhombohedral shaped) of about 12 nm were found.

Differently, in Cs5 the fibrils are smaller (55 nm × 3 nm) than the other materials. These reduced dimensions and the absence of the nanometric plaque-like regions may be related with the noticeable differences in the textural properties as discussed above, in comparison with the other Al_2O_3–TiO_2 materials. In other words, the intercrossing degree and disorder among the fibers (interfibrillar porosity) as well as their length may cause the non-uniform pore size distributions which extend up to ∼100 nm as indicated in Fig. 2.

Another difference among the samples is the presence of surface nanoparticles on the fibrils and/or mixed with them, particularly in the case of Ds5. In order to clear out the nature of these particles, a magnified TEM of both the plaque-like nanoparticles region and the fibril region were taken and the corresponding selected area electron diffraction (SAED) patterns were taken (see Fig. 5). In SAED pattern from the plaque-like region (Fig. 5(a)) shows very well-defined rings representing the characteristic planes 1 0 1 and 2 1 1 of anatase TiO_2 in combination with those of γ-alumina [17,18]. The SAED pattern (Fig. 5(b)) of the highly fibrillar region showed faint rings from the 1 0 1 and 2 1 1 of anatase in combination with those of γ-alumina [19,20]. These results indicate that fibrillar populations in Ds5 and Sd5 samples have low crystallinity and that they are mainly made up of γ-alumina and very likely, anatase particles on top. In the case of Cs5 (Fig. 5(c)), SAED pattern point out that this material is solely composed of γ-alumina and TiO_x species may be very well dispersed within the fibrils.

XRD patterns in Fig. 6 agree very well with the SAED results, showing γ-alumina phase in all samples (specifically 4 4 0, 4 0 0 and 3 1 1 planes), besides of TiO_2 anatase phase in some samples (more intense peak in 1 0 1 plane on 25.5° at 2θ axis). Particularly, the material obtained by deposition (Ds5) displayed the highest intensity of the five characteristic peaks of anatase phase (plane 1 0 1 is the most intense and representative). Sample Sd5, obtained by stepwise deposition had an intermediate intensity in comparison with those of Cs5 and Ds5 samples and showed XRD patterns with anatase peaks for 1 0 1 and 2 1 1 planes only. Co-precipitated sample, Cs5, showed an XRD pattern with the least intensity, in which only a faint 1 0 1 peak was observed. The intensity and width difference in the 1 0 1 plane for three Al_2O_3–TiO_2 mixed oxides indicate generation of different anatase crystallite sizes. A higher peaks intensity of alumina in Ds5 and Sd5 samples in comparison with those in Cs5 and A6pHs single alumina, suggests a better Al_2O_3 crystallinity in Ds5 and Sd5 samples.

Raman spectroscopy is a very sensitive technique for TiO_x compound identification [21]. Raman spectra of fibrillar Al_2O_3–TiO_2 materials, obtained for three different titania incorporation methods, are shown in Fig. 7. The sample based on titania deposition (Ds5) showed clear and intense Raman signals typical of anatase phase at 145, 199, 399, 520 and 644 cm^{-1} [21]. This result strongly indicates that anatase phase is segregated in considerable amount in this sample, in agreement with XRD and TEM results. On the other hand, co-precipitated Cs5 alumina–titania showed only a small shoulder in the place where the most intense anatase Raman signal appears (146 cm^{-1}) and most of the spectra is made up of a fluorescence signal typical of polymerized and isolated Ti–O–Al bonds in a bulk of mixed oxide [13]. Then, in the case of Cs5, Raman results indicate the co-existence of (i) anatase crystallites on the surface of the fibrils and (ii) TiO_x embedded in the bulk of the Al_2O_3–TiO_2 fibrils. Sd5 sample, similar to Cs5, showed the anatase signal at 145 cm^{-1}, but being more prominent than that in Cs5, and other anatase peaks at 521 and 645 cm^{-1}, in spite of the strongest fluorescence among all samples in Fig. 7. According to Gutierrez-Alejandre et al. the strong fluorescence in Al_2O_3–TiO_2 materials implies that TiO_x species are embedded in the bulk of alumina [22]. A similar explanation applies to Sd5 material; being in agreement with SAED and XRD results, and considering that alumina fibrils are practically uncovered by anatase particles. It is worth to mention that until recently alumina material were considered very fluorescent materials and Raman futures were thus undisclosed, however there are a few works that identify the Raman signals of alumina [23], the most characteristic bands appearing at 362 and 496 cm^{-1}. In a recent study Zhu et al. [24]

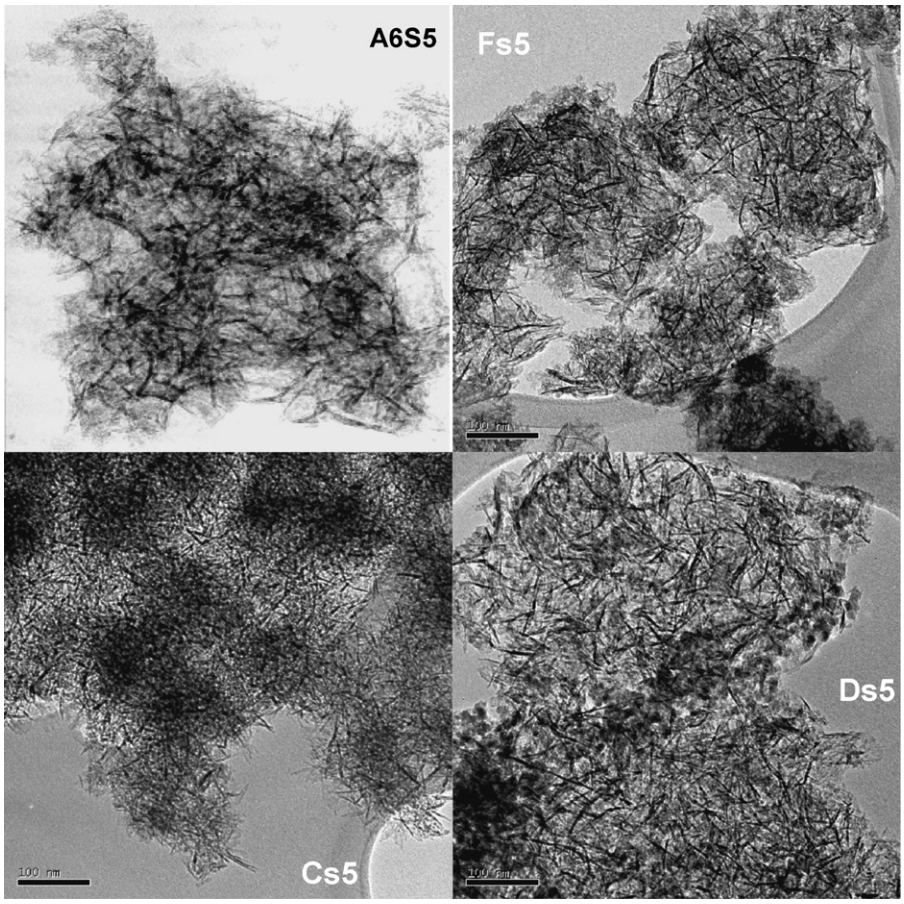

Fig. 4. TEM images that show the fibrillar morphology of single A6pHs alumina and alumina–titania materials calcined at 500 °C.

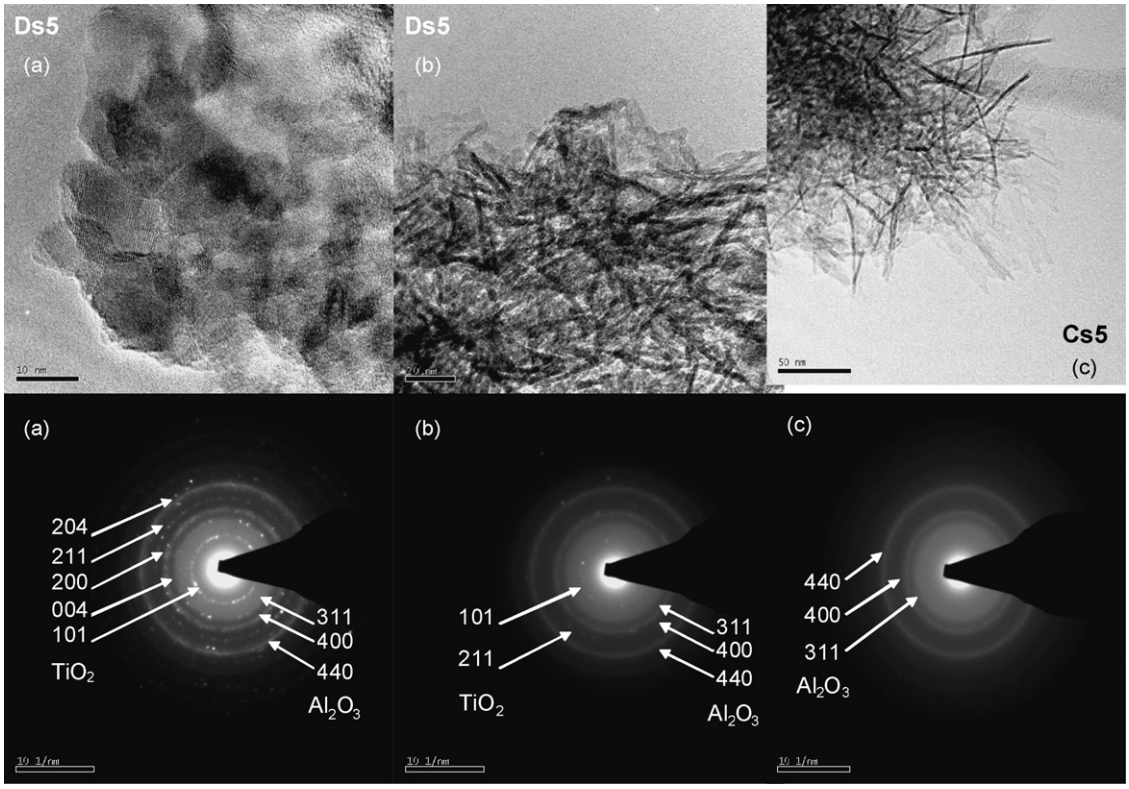

Fig. 5. TEM images and SAED patterns of A6pHs, Ds5 and Cs5 samples.

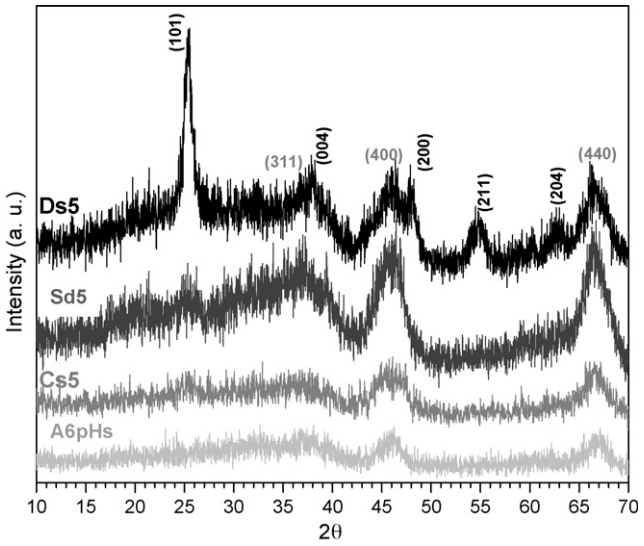

Fig. 6. Wide-angle XRD patterns of single A6pHs alumina and those of alumina–titania materials calcined at 500 °C.

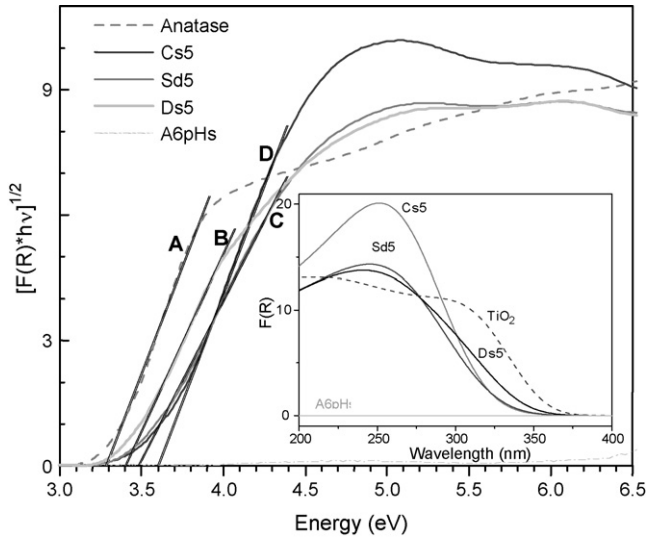

Fig. 8. UV–vis diffuse reflectance spectra and band gap energy (inset): (A) anatase, E_g = 3.3 eV; (B) Ds5, E_g = 3.4 eV; (C) Sd5, E_g = 3.5 eV; (D) Cs5, E_g = 3.6 eV.

reported that there is a direct correlation between the presence and intensity of Raman signals and the boehmite nanofibrillar morphology. The two Raman bands in A6pHs (see Fig. 7) are in agreement with Zhu results.

UV–vis diffuse reflectance spectra of fibrillar Al_2O_3–TiO_2 materials and reference fibrillar alumina are shown in Fig. 8; calculated band gap energy spectra are included on inset of Fig. 8. Band gap energy (E_g) was obtained by the abscise interception in $h\nu$ *vs.* $[F(R)h\nu]^{1/2}$ on the plot. $F(R)$ is Kubelka–Munk function for one infinite thickness layer and $h\nu$ is the incident foton's energy. The E_g values were: anatase = 3.3 eV, Ds5 = 3.4 eV, Sd5 = 3.5 eV and Cs5 = 3.6 eV. E_g increase as aluminas–titanias behave less like as semiconductor [25].

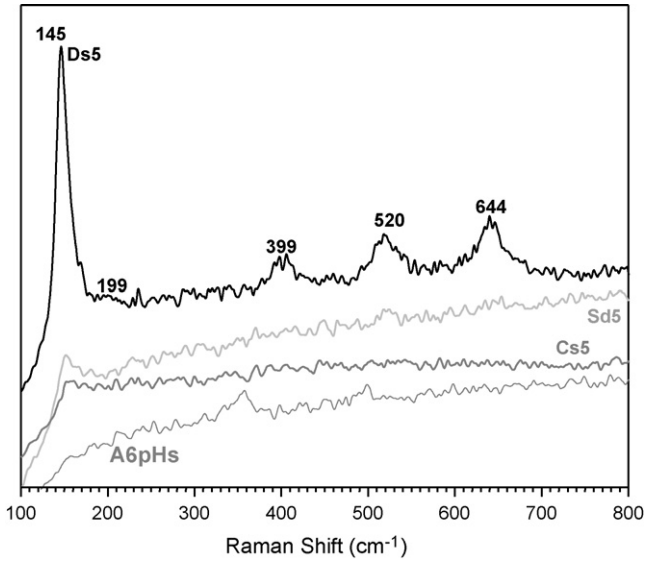

Fig. 7. Raman spectra patterns of single A6pHs alumina and those of alumina–titania materials calcined at 500 °C.

4. Conclusions

The three different ways to incorporate titanium oxysulfate combined with a pH-swing method yielded nanofibrillar alumina–titania materials, but with a clear different titania dispersion depending on the incorporation method of the Ti compound. The deposition procedure resulted in considerably segregated anatase particles on the surface and /or occluded in the inter-fibrillar pores. In comparison stepwise deposition formed less segregated anatase particles. The co-precipitation procedure yielded very small anatase crystallites, very highly dispersed or embedded on/in the fibrils. In the three alumina–titania systems only one TiO_2 phase was detected: anatase. In the end, Al_2O_3–TiO_2 nanofibrillar systems were obtained by a pH-swing method, with specific surface areas higher than 300 m^2/g, and pore volumes equal or higher than 1 cm^3/g, after calcining at 500 °C; maintaining its fibrillar morphology below this temperature.

References

[1] S. Iijima, Nature 354 (1991) 56.
[2] J.H. Fendler, F.C. Meldrum, Adv. Mater. 7 (1995) 607.
[3] C. Kresge, M. Leonowicz, W. Roth, J. Vartuli, J. Beck, Nature 359 (1992) 710.
[4] S. Inagaki, Y. Fukushima, K. Kuroda, Chem. Commun. (1993) 680.
[5] H.Y. Zhu, J.D. Riches, J.C. Barry, Chem. Matter. 14 (2002) 2028.
[6] M. Fuji, Y. Sugiyama, T. Takei, M. Chikazawa, K. Tanabe, K. Mitsuhashi, J. Soc. Powder Technol. 39 (2002) 102.
[7] J. Wang, L. Dong, Y. Hu, G. Zheng, Z. Hu, Y. Chen, J. Solid State Chem. 157 (2001) 274.
[8] Z. Ying, B. Gevert, J. Otterstedt, J. Sterte, Appl. Catal. A 153 (1997) 69.
[9] J. Escobar, A. De los Reyes, T. Viveros, Ind. Eng. Chem. Res. 39 (2000) 666.
[10] J. Ramirez, A. Gutierrez-Alejandre, J. Catal. 170 (1997) 108.
[11] C. Contescu, A. Contescu, Chem. Rev. 95 (1995) 477.
[12] A. Gutierrez-Alejandre, M. Gonzalez-Cruz, M. Trombetta, G. Busca, J. Ramirez, Micropor. Mesopor. Mater. 23 (1998) 265.

[13] J. Ramirez, G. Macias, L. Cedeño, A. Gutierrez-Alejandre, R. Cuevas, P. Castillo, Catal. Today 98 (2004) 19.
[14] J.A. Muñoz-López, Master grade thesis, México D.F., Universidad Autónoma Metropolitana Azcapotzalco, 2003.
[15] T. Ono, Y. Ohguchi, O. Togari, Preparation of Catalysts III, Wiley, New York, 1983 , p. 383.
[16] G. Ertl, H. Knozinger, J. Weitkamp, Handbook of Heterogeneous Catalysis, vol. 4, Wiley–VCH, 1999,, p. 1804.
[17] A. Weibel, R. Bouchet, F. Boulch, P. Knauth, Chem. Mater. 17 (2005) 2378.
[18] D. Li, J. McCann, M. Gratt, Y. Xia, Chem. Phys. Lett. 394 (2004) 387.
[19] G. Ennas, A. Falqui, G. Paschina, G. Marongiu, Chem. Mater. 17 (2005) 6486.
[20] J. Aguado, M. Escola, C. Castro, B. Paredes, Micropor. Mesopor. Mater. 83 (2005) 181.
[21] J. Ramirez, P. Rayo, A. Gutierrez-Alejandre, J. Ancheyta, M. Rana, Catal. Today 109 (2005) 54.
[22] A. Gutierrez-Alejandre, M. Gonzalez-Cruz, R. Trombetta, G. Busca, J. Ramirez, Micropor. Mesopor. Mater. 23 (1998) 265.
[23] C. Doss, R. Zallen, Phys. Rev. B 48 (1993) 21.
[24] H.Y. Zhu, X.P. Gao, D.Y. Song, Y.Q. Bai, S.P. Ringer, Z. Gao, Y.X. Xi, W. Martens, J.D. Riches, R.L. Frost, J. Phys. Chem. B 108 (2004) 4245.
[25] S. Lee, C. Jeon, C. Park, Chem. Mater. 16 (2004) 4292.